

Exploring accretion disc physics and black hole growth with regular monitoring of ultrafast AGN winds

Ken Pounds, Andrew Lobban and Chris Nixon

Department of Physics and Astronomy, University of Leicester, Leicester LE1 7RH UK

Received September 2016, accepted December 2016

Key words galaxies:active - galaxies:Seyfert;quasars:general - galaxies:individual:PG1211+143 - X-ray:galaxies

15 years of *XMM-Newton* observations have established that ultra-fast, highly ionized winds (UFOs) are common in radio-quiet AGN. A simple theory of Eddington-limited accretion correctly predicts the typical velocity ($\sim 0.1c$) and high ionization of such winds, with observed flow energy capable of ejecting star-forming gas. An extended *XMM-Newton* observation of the archetypal UFO, PG 1211+143 recently found a more complex flow pattern, suggesting that intensive *XMM-Newton* observations offer exciting potential for probing the inner accretion disc structure and SMBH growth.

© 2017 WILEY-VCH Verlag GmbH & Co. KGaA, Weinheim

1 Introduction

X-ray spectra from an *XMM-Newton* observation of the luminous Seyfert galaxy PG 1211+143 in 2001 provided the first detection of strongly blue-shifted absorption lines of highly ionized gas in a non-BAL Active Galactic Nucleus (AGN), corresponding to a sub-relativistic outflow velocity of $\sim 0.1c$ (Pounds et al. 2003), later adjusted to $0.15 \pm 0.01c$ with the identification of additional absorption lines and broad-band spectral modelling (Pounds & Page 2006). Further observations of PG 1211+143 over several years with *XMM-Newton*, *Chandra* and *Suzaku* found the high velocity outflow to be persistent but of variable strength (Reeves et al. 2008). Evidence that the outflow in PG 1211+143 was both massive and energetic - with potential importance for galaxy feedback (King 2003, 2005) - came from the detection of a P-Cygni line profile and other broad emission features by combining the 2001, 2004 and 2007 *XMM-Newton* EPIC spectra (Pounds & Reeves 2009). Examination of archival data from *XMM-Newton* and *Suzaku* has since shown ultra-fast, highly-ionized outflows (UFOs) to be common in nearby, luminous AGN (Tombesi et al. 2010, 2011; Gofford et al. 2013). The frequency of these detections suggest a wide angle outflow, with mass rate and kinetic energy in a persistent wind capable of curtailing star formation and black hole growth (Pounds 2014), and providing the link between black hole and stellar bulge masses implied by the observed $M - \sigma$ relationship (Gebhardt et al. 2000; Ferrarese & Merritt 2000).

An extended *XMM-Newton* observation of PG 1211+143 in 2014 has now provided uniquely high quality X-ray spectra of PG 1211+143, revealing previously unseen velocity structure in the ~ 6 – 10 keV energy band. Spectral modelling of data from the high-energy pn camera (Strueder et al. 2001) identified the observed absorption lines with resonance and higher order transitions of highly-

ionized Fe, consistent with two distinct outflow velocities $v \sim 0.066c$ and $v \sim 0.13c$ (Pounds et al. 2016a: hereafter P16).

In that first report of a dual velocity, primary (high column) wind it was suggested that the simultaneous observation of two ‘Eddington Winds’ (King & Pounds 2015) might be evidence of ‘chaotic accretion’, where a clump of matter approaching the black hole divides to form prograde and retrograde accreting flows, with a corresponding difference in accretion efficiency and potential wind velocity. Marginal evidence in P16 for a third velocity component ($v \sim 0.19c$) has since been supported in an analysis of the higher resolution soft X-ray spectra from the Reflection Grating Spectrometer (RGS; den Herder et al. 2001) during the same 2014 *XMM-Newton* observation (Pounds et al. 2016b). Here we discuss that further challenge to the simple Eddington Wind model and suggest that future well-sampled observations of a powerful UFO, as observed in PG 1211+143, have exciting potential to study the accretion physics determining how the super-massive black hole (SMBH) continues to grow in the interval between mergers.

2 Eddington Winds

The ‘Black Hole Winds’ model (King & Pounds 2003) provides a simple physical basis for high velocity outflows in AGN accreting at or above the Eddington limit, and has the bonus of useful predictive power.

Based on the initial observation of PG 1211+143 the model assumes a primary (high column) wind will have electron scattering optical depth $\tau \sim 1$, measured inwards from infinity to a distance of order the Schwarzschild radius. Since on average every photon emitted by the AGN scatters about once before escaping to infinity, and gives up all its momentum to the wind, the total (scalar) wind momentum

arXiv:1609.05674v2 [astro-ph.GA] 23 Jan 2017

will be of order the photon momentum. Equating the wind and photon momenta then gives:

$$\dot{M}_w v \simeq \frac{L_{\text{Edd}}}{c}, \quad (1)$$

where \dot{M}_w and v are the mass rate and velocity in the wind and L_{Edd} is the Eddington luminosity. For accretion from a disc, as here, the classic paper of Shakura & Sunyaev (1973) finds a similar result at super-Eddington mass inflow rates, with the excess accretion being expelled from the disc in a quasi-spherical wind. Since the Eddington accretion rate is:

$$\dot{M}_{\text{Edd}} = \frac{L_{\text{Edd}}}{\eta c^2}, \quad (2)$$

the Eddington wind terminal velocity is then:

$$v \simeq \frac{\eta}{\dot{m}} c \sim 0.1c, \quad (3)$$

where \dot{m} is the accretion ratio, typically of order unity in SMBH growth episodes, as relevant here (see Section 3 of King & Pounds 2015 for a further discussion).

Assuming the wind is launched and then coasts, the observed outflow velocity will be of order the escape velocity at the launch radius, providing a potential probe of the accretion geometry from observation of the wind profile. For PG 1211+143, wind velocity components of $v \sim 0.13c$ and $v \sim 0.066c$ correspond to $R_{\text{launch}} \sim 60R_s$ and $\sim 240R_s$, respectively. For a SMBH mass of $3 \times 10^7 M_\odot$ (Kaspi et al. 2000) and $R_s = 2GM/c^2$, the respective launch radii are then $\sim 4 \times 10^{14}$ cm and $\sim 1.6 \times 10^{15}$ cm.

From King & Pounds (2015) we also note the ionization parameter of the wind:

$$\xi = \frac{L_i}{NR^2} \quad (4)$$

essentially determines which spectral lines are observed. Here $L_i = l_i L_{\text{Edd}}$ is the ionizing luminosity, with $l_i < 1$ specified by the AGN spectrum, and $N = \rho/\mu m_p$ the number density of the UFO gas. Assuming mass conservation in the wind the ionization parameter is then:

$$\xi = 3 \times 10^4 \eta_{0.1}^2 l_2 \dot{m}^{-2} = 3 \times 10^4 v_{0.1}^2 l_2 \quad (5)$$

where $l_2 = l_i/10^{-2}$, and $\eta_{0.1} = \eta/0.1$.

Powerful AGN winds are therefore most likely to be observable in the X-ray spectrum, and by current instruments such as the pn and MOS cameras on *XMM-Newton*

Figure 1 summarises data from the 35 best-determined UFOs from the *XMM-Newton* and *Suzaku* archival searches, showing a distribution of wind velocity and ionization parameter consistent with the above predictions of an Eddington wind. We suggest in the remainder of this paper that by using the wind velocity as a marker of the region in the disc where the accretion rate first exceeds the Eddington rate, well sampled observations of UFOs over the next decade of *XMM-Newton* could provide direct observational constraints on the detailed way in which a SMBH grows between mergers.

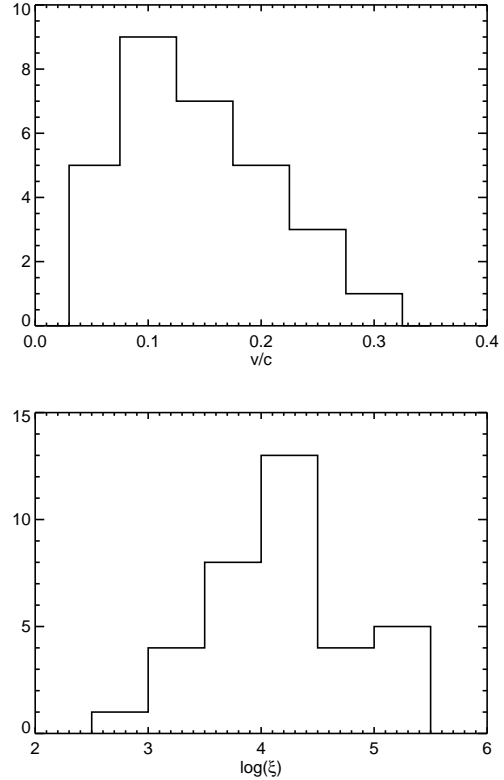


Fig. 1 Distribution of primary outflow velocity and ionization parameter in 35 radio-quiet AGN with UFOs detected in the *XMM-Newton* or *Suzaku* archival surveys. The observed properties are consistent with the predictions of an Eddington wind.

2.1 The origin of a unique wind velocity

As noted above, Shakura & Sunyaev (1973) first pointed out that a black hole supplied with matter at a super-Eddington rate will expel matter from its accretion disc so as to never exceed the local Eddington luminosity.

In such a situation, which should be relevant to a luminous AGN such as PG 1211+143, where a comparison of bolometric luminosity and black hole mass indicates a mean accretion rate close to the Eddington rate, it is interesting to follow a clump of additional matter moving inwards on the local viscous timescale.

While the disc successfully radiates accretion energy at large disc radii and there is no wind, a critical point arises where the local accretion luminosity reaches the Eddington rate. This defines the Eddington radius (R_{Edd}), where

$$R_{\text{Edd}} = \frac{\dot{m}GM}{L_{\text{Edd}}}. \quad (6)$$

The wind starts at R_{Edd} , with the correct (local escape) velocity. Mass loss from within this radius falls quickly, since the local accretion rate $\dot{M}(R)$ will scale so as to keep $GM\dot{M}(R)/R \simeq L_{\text{Edd}}$, and $\dot{M}(R) \propto R$. Hence there is less absorption from smaller radii which may show as a higher

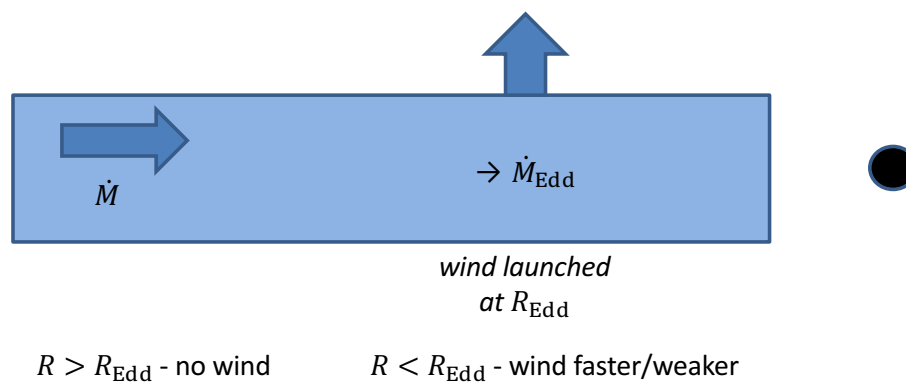


Fig. 2 Cartoon depicting the inflow of an incident of enhanced accretion. On reaching a critical radius in the disc where the accretion rate exceeds the local Eddington rate a fast wind is launched, as described in the text. While there is no wind at larger radii, inwards of R_{Edd} a weaker, higher velocity wind might be seen.

velocity wing to the primary outflow. Figure 2 illustrates the inflow of such an incident of enhanced accretion.

Observation of primary (high column) wind components with different UFO velocities in PG 1211+143 suggests that this simple picture of a flat axisymmetric disc does not always apply. As noted in Section 1, P16 reported the detection of two simultaneous primary outflow velocities and speculated that the dual velocities identified in the high quality Fe K absorption spectrum might be explained by ‘chaotic accretion’ (King & Pringle 2006), consisting of many prograde and retrograde events. The former would remain stable to smaller radii, thereby releasing more gravitational energy, a higher accretion efficiency, η , and a higher launch velocity than the retrograde flow, for $\dot{m} \sim 1$.

It is interesting to note a recent study of accreting filaments close to Sgr A* showing how an accreting cloud might divide on approach to the black hole (Lucas et al. 2013), with the potential to produce prograde and retrograde accretion flows. While X-ray monitoring of AGN winds is at present too limited to show how common such dual velocities winds might be. Meanwhile, a still more complex picture is emerging, with the recent confirmation of a third high velocity component in the primary wind from PG 1211+143.

In Section 3 we review the current observational evidence; then in Section 4 we briefly consider how such a multiple velocity primary (high-column) wind might result where an accreting ‘cloud’ approaches the disc at an oblique angle to the black hole spin plane, causing the inner disc to warp and break up. We suggest such a ‘breaking disc’ (Nixon et al. 2012) could launch multiple winds when fragments of the warped inner disc collide and cool, with the possibility of near-radial infall creating new regions of super-critical accretion. Since the pattern of wind velocities corresponds to the geometry of such accretion structure, we suggest that future well-sampled observations of powerful AGN winds could provide unique information on the complexities of SMBH accretion in the lengthy interval between mergers.

3 Complex velocity structure in the powerful ionized wind of the luminous narrow line Seyfert galaxy PG 1211+143

Given the important implications for AGN accretion and galaxy feedback, pioneered by *XMM-Newton* observations, a more extended study of PG 1211+143 was carried out over the period 2014 June 2 to July 9, seeking to provide greater detail on the spectral and dynamical structure of the outflow. The resulting low background exposure of 545 ks was an order of magnitude greater than for the any of the previous *XMM-Newton* observations of PG 1211+143 in 2001, 2004 and 2007, and significantly more than for any other UFO to date. The high statistical quality of the 2014 observation has revealed a more complex absorption structure than previously seen in the Fe K spectrum, providing strong evidence of multiple wind components.

Figure 3 (top panel) shows the relevant section of the stacked pn camera data plotted as a ratio to the continuum. The emission near 6 keV is now resolved, with component rest energies close to the neutral Fe K fluorescent emission line and the 1s–2p resonance emission lines of He-like and H-like Fe. The absorption line at ~ 6.9 keV, dominant in 2001, is now a factor ~ 3 weaker, with an equivalent width of 47 ± 7 eV. However, the much longer exposure in 2014 reveals additional absorption structure, with significant absorption lines at ~ 6.6 , ~ 6.9 , ~ 7.3 , ~ 7.5 , ~ 7.8 , ~ 8.2 and ~ 8.7 keV.¹

While most previous UFO detections have been based on the identification of one - or at most two - blue-shifted absorption lines, the high quality of the 2014 PG 1211+143 data warranted more detailed modelling of the spectral features. This was done in P16 by including both absorption and emission spectra from ionized circumnuclear gas, mod-

¹ The absorption lines at ~ 8.2 and ~ 8.7 keV lie close to fluorescent X-ray emission lines of Cu and Zn arising from energetic particle impacts on the pn camera electronics board (Strueder et al. 2001). Fortunately, the very low particle background throughout most of the 2014 *XMM-Newton* observations ensured such background features have a negligible effect on the source spectrum.

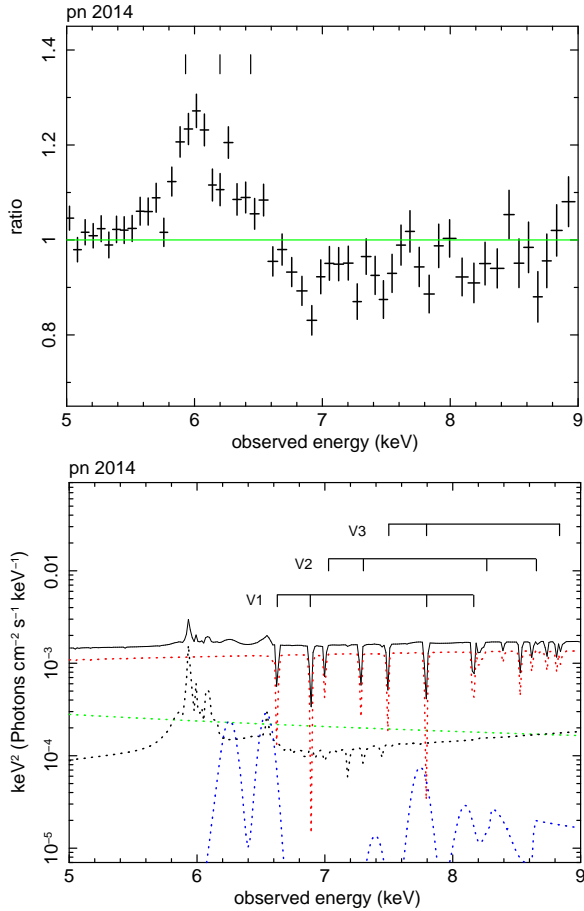


Fig. 3 Top: Fe K emission and absorption profile in the stacked 2014 pn spectrum showing a weaker absorption line at ~ 7 keV compared with 2001, but additional absorption structure at higher energy and emission components at a small blueshift relative to markers indicating the rest energies of Fe K emission lines of neutral, He-like and H-like ions, respectively. Lower: XSTAR model fit including three highly ionized absorption components. Colour coding is blue for the high-ionization emission, with the ionized reflection continuum and Fe K fluorescence line shown in black. The hard power law and unabsorbed power law components are in red and green, respectively.

elled with grids of pre-computed spectra based on the XSTAR code (Kallman et al. 1986).

Continuum reflection was also included in the P16 modelling in order to account for an Fe K absorption edge that could - if ignored - result in the line series absorption above ~ 7 keV being overstated. Resolution of the Fe K fluorescence line, a common feature in AGN spectra, physically linked with continuum scattering (or ‘reflection’) from dense matter illuminated by the nuclear hard X-ray source (Nandra & Pounds 1994), was used to constrain the level of continuum reflection. That constraint was made by adding a XILLVER component (Garcia et al. 2013) to the spectral model, finding a reflection factor having only a small effect on the derived column densities of the absorption compo-

nents. Figure 3 (lower panel) shows a broad and shallow ionized reflection edge in the best-fit spectral model.

Separate absorption spectra were required in P16 to match the observed spectral structure, with XSTAR parameters corresponding to highly ionized outflows at $\sim 0.13c$ and $\sim 0.066c$, comprising the dual velocity wind reported there. The lower panel of Figure 3 shows how the principal absorption transitions in the dual velocity absorber model (v1 and v2) match 6 of the 7 strongest absorption lines in the stacked pn data. In particular, absorption lines at ~ 7.0 , ~ 7.3 , ~ 8.2 and ~ 8.7 keV correspond to α (resonance) and β transitions in Fe XXV and Fe XXVI for a velocity of $0.129 \pm 0.002c$, while absorption lines at ~ 6.6 , ~ 6.9 , ~ 7.8 and ~ 8.2 keV match the same four ionic transitions, but for the substantially lower outflow velocity of $0.066 \pm 0.003c$.

The photoionized emission in the model is seen in Figure 3 to match emission features in the data, the two high energy components being identified with the He- and H-like resonance lines, in a ratio set by the ionization parameter. The Fe Lyman- β emission line can also be seen in both data and model at ~ 7.7 keV, with a similar blueshift.

The potential of stable pn camera data of high statistical quality to resolve and interpret such complex spectra (notwithstanding the limited detector energy resolution: ~ 150 eV at 6 keV), in combination with physically realistic modelling, is demonstrated by the strong preference for a second outflow velocity in P16. The dual velocity model is illustrated in the lower panel of Figure 3, where the Lyman- α line of the lower velocity flow (v1) blends with He- α from the higher velocity wind (v2) to form the observed broad absorption feature near 7 keV, while the He- α line for the lower velocity outflow is now seen to have been partly hidden by the emission line at ~ 6.5 keV. A further outcome of the blend at ~ 7 keV is to increase the relative strength of the higher velocity Lyman- α line and hence the ionization parameter and column density of that flow component.

3.1 Evidence for a third outflow component

Since the report of the dual velocity primary outflow was published in P16, a corresponding analysis of the soft X-ray spectral data from the *XMM-Newton* RGS has been completed (Pounds et al. 2016b), finding counterparts of both dual velocity absorbers, as well as a higher velocity outflow at $0.188 \pm 0.002c$. The confirmation of 3 velocity components in higher-resolution spectra provides strong support for the modelling of the higher-energy spectra, while revealing the presence of co-moving, higher density matter in each flow component, which - being less highly ionized - retains significant opacity in the soft X-ray band.

Adding a third highly-ionized absorber to the dual velocity model of P16, with velocity $v \sim 0.19c$, provides a match to the seventh observed absorption line, at ~ 7.5 keV. The corresponding absorption series v3 in the lower panel of Figure 3 shows the Fe Lyman- α and Fe He- α resonance

Table 1 Parameters of the highly-ionized outflow obtained from a 2–10 keV spectral fit to the 2014 pn data, with 3 photoionized absorbers, defined by ionization parameter ξ (erg cm s^{-1}), column density N_{H} (cm^{-2}) and outflow velocity (v/c), together with a photoionized emission spectrum modelled by an ionization parameter and outflow velocity. Extracted or added luminosities for each photoionized component are for 2–10 keV.

Comp.	$\log \xi$	$N_{\text{H}}(10^{23})$	v/c	$L_{\text{abs/em}}$
abs 1	3.5 ± 0.1	2.6 ± 1.3	0.067 ± 0.003	11×10^{41}
abs 2	3.9 ± 0.6	1.5 ± 1.0	0.129 ± 0.006	6×10^{41}
abs 3	3.4 ± 0.2	0.5 ± 0.5	0.187 ± 0.003	3×10^{41}
emission	3.5 ± 0.1	0.1(f)	0.015 ± 0.006	6×10^{41}

absorption lines matching the observed spectral features at ~ 7.5 keV and ~ 7.8 keV, respectively, with the latter blending with the (weaker) Ly- β line in the v2 series. In addition the Lyman- β line of v3 now blends with the He- β at v2 to make a better match to the strong absorption at ~ 8.7 keV.

The simultaneous detection of 3 primary, highly ionized velocity components (Table 1) raises a further challenge to the Eddington Winds model for the simple axisymmetric accretion disc envisaged in Section 2.1. We discuss in Section 4 how such further complexity might arise.

4 Disc tearing

In general an accretion disc around a black hole orbits in a plane misaligned to the spin of the central black hole. This is particularly relevant to AGN accretion where gas in the galaxy falls from far outside the radius of gravitational influence of the central SMBH. In this case gas is likely to fall in with essentially random orientations (King & Pringle 2006, 2007). When misaligned to the black hole spin, the disc is subject to Lense-Thirring precession which causes misaligned orbits to precess around the black hole spin vector. This effect is strongly radially dependent with orbits at smaller radii precessing faster. As the orbits precess, the disc warping is communicated radially by an oscillating radial pressure gradient around the orbit which resonates with the epicyclic motion giving a strong torque which acts faster than the usual viscous accretion torque (Papaloizou & Pringle 1983; Ogilvie 1999; Nixon 2015). This effective viscosity communicating the warp through the disc, combined with the precession from the spinning black hole results in an aligned inner disc connected to a misaligned outer disc by a smooth warped region (Bardeen & Petterson, 1975).

This picture relies on the assumption that the internal disc communication is sufficiently fast that the disc can communicate the precession as it is occurring. However, close to the black hole, the precession can approach the dynamical timescale. For a black hole spin, a , and black hole gravitational radius, $R_{\text{g}} = GM/c^2$, the precession frequency is $\Omega_{\text{p}} = 2a(R_{\text{g}}/R)^3 c^3/GM$. Thus for spins of or-

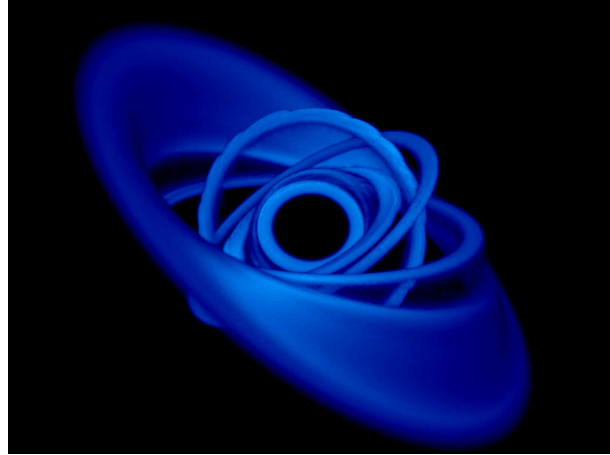


Fig. 4 A disc misaligned to the central black hole spin, which has been torn apart. The innermost region is aligned to the black hole spin. Outside this the disc has been torn into discrete rings by the strong Lense-Thirring precession. Further out, the disc can communicate the precession efficiently and thus shows a smooth warp. Between precessing rings, the material shocks and loses rotational support, falling inwards to increase the instantaneous accretion rate, potentially above the local Eddington limit, thus expelling a new wind.

der unity, close to the black hole the precession can be so rapid that it is unlikely that the disc warp can be communicated efficiently in all cases. If the disc is unable to communicate the precession, then we expect the disc to break up into independently precessing rings of gas. Nixon et al. (2012) derive an approximate radius in the disc inside which this can occur (see also Nealon et al. 2015, 2016; Dogan et al. 2015). For typical AGN disc parameters this can be out to a few hundred gravitational radii from the black hole. Nixon & Salvesen (2014) discuss this model in the context of X-ray binary state transitions. A typical tearing disc structure is shown in Figure 4.

As the disc breaks up into discrete rings, each ring precesses on its own timescale. After a time, two neighbouring rings precess such that their orbital velocities become partially opposed at the contact points. This causes shocks and internal cancellation of disc angular momentum: while the system's total angular momentum is conserved, the disc has borrowed angular momentum from the hole to cancel its own. The shocked material has now lost rotational support and falls inwards to a new radius defined by its residual angular momentum where - if it can cool fast enough - it forms a new disc. The material added to the inner disc from the 'disc-tearing' region can result in a dramatic increase in the local accretion rate, allowing an otherwise sub-Eddington flow to become super-Eddington for a short time, with the launch of winds over timescales of order days (for radii of order $10R_{\text{g}}$) to years (for radii of order $100R_{\text{g}}$), assuming a $3 \times 10^7 M_{\odot}$ black hole with near-maximal spin.

This scenario illustrates how the fast outflow properties of an AGN may be intimately linked with the inner accretion disc physics. Detailed observations with high cadence and resolution could then provide stringent constraints on accretion disc models and provide the opportunity to distinguish between models and refine current understanding of these systems, which are integral to much of modern astronomy.

5 Discussion

The extended *XMM-Newton* observation of PG 1211+143 in 2014 provided uniquely high quality hard X-ray spectra of this archetypal UFO, revealing previously unseen structure in the $\sim 6\text{--}10$ keV energy band. Spectral modelling has identified the observed absorption structure with line series of H- and He-like Fe, consistent with three distinct outflow velocities. The analysis is a strong demonstration of the power of modelling UFOs with grids of pre-computed absorption spectra, which take proper account of all absorption line and continua effects.

Given the success of the Black Hole Winds model (King & Pounds 2003) in predicting the group properties of UFOs, we consider the more complex velocity structure in the same context. The properties of such ‘Eddington winds’ are described in greater detail in King & Pounds (2015), which includes a discussion on the observability of UFOs as they evolve from being optically thick at launch to transparency after radial expansion. For winds launched in the inner accretion disc the visibility timescale for high velocity winds can be on order months or less. That view is supported by a review of the recent archival searches (Tombsi et al. 2011; Gofford et al. 2013), leading King & Pounds (2015) to suggest that currently observed AGN winds are more likely to be composed of sporadic, quasi-spherical shells, than a continuous outflow, with only the most recently launched shells remaining visible.

Considering the new 2014 observation of PG 1211+143 in that context, in P16 we suggested the $v \sim 0.066c$ and $v \sim 0.13c$ outflows represent recently launched shells, corresponding to local super-Eddington episodes from prograde and retrograde accretion, with the higher efficiency of the former (due to the inflow remaining stable to a smaller radius) yielding the higher wind velocity (ref. equation 3).

The simultaneous detection of 3 primary wind velocities now suggests a still more complex picture, and in Section 4 we note that multiple ‘accretion dumps’ at different regions in the inner disc, leading to corresponding wind launches, might arise from disc warping (and breaking) due to the Lense-Thirring effect (Nixon et al. 2012). Monitoring the resulting pattern of disc winds over the next decade of *XMM-Newton* observations offers the exciting prospect of constraining detailed models of accretion and black hole growth.

While the robustness of the dual velocity absorption model described in P16, implying line resolution comparable with the intrinsic energy resolution of the pn camera,

was an indication of what can be achieved with data of high statistical quality and from a well calibrated and stable detector, higher resolution data remain vital for observation and interpretation of more complex outflows. Combination of the EPIC and RGS instruments will remain important in *XMM-Newton* observations of AGN outflows in the years ahead. With the unfortunate loss of the *HITOMI* spacecraft, that approach is likely to remain the best opportunity to explore accretion physics and black hole growth by intensive mapping of powerful AGN available prior to the launch of *Athena*.

Acknowledgements. The continuing guidance of our colleague Andrew King is gratefully acknowledged by the authors. *XMM-Newton* is a space science mission developed and operated by the European Space Agency and we acknowledge in particular the excellent work of ESA staff in Madrid in successfully planning and conducting the observations of PG 1211+143. The UK Science and Technology Facilities Council funded the postdoctoral research assistantship of AL and an Ernest Rutherford Fellowship for CN (ST/M005917/1).

References

- Bardeen J.M. & Petterson J.A. 1975, *ApJ*, 195, L65
 den Herder J.W. et al. 2001, *A&A*, 365, L7
 Dogan S., Nixon C., King A.R., Price D.J. 2015, *MNRAS*, 449, 1251
 Ferrarese L. & Merritt D. 2000, *ApJ*, 539, L9
 Garcia J. et al. 2013 *ApJ*, 768, 146
 Gebhardt K. et al. 2000, *ApJ*, 539, L13
 Gofford J., Reeves J.N., Tombsi T., Braito V., Turner T.J., Miller L., Cappi M. 2013, *MNRAS*, 430, 60
 Kallman T., Liedahl D., Osterheld A., Goldstein W., Kahn S. 1996, *ApJ*, 465, 994
 Kaspi S. et al. 2000, *ApJ*, 533, 631
 King A.R. & Pounds K.A. 2003, *MNRAS*, 345, 657
 King A.R. 2003, *ApJ*, 596, L27
 King A.R. 2005, *ApJ*, 635, L121
 King A.R. & Pringle J.E. 2006, *MNRAS*, 373, 90
 King A.R. & Pringle J.E. 2007, *MNRAS*, 377, 25
 King A.R. & Pounds K.A. 2015, *ARA&A*, 53, 115
 Lucas W.E., Bonnell I.A., Davies M.B., Rice W.K.M. 2013, *MNRAS*, 433, 353
 Nandra K. & Pounds K.A. 1994, *MNRAS*,
 Nealon R., Price D.J., Nixon C. 2015, *MNRAS*, 448, 1526
 Nealon R., Price D.J., Nixon C., King A.R. 2016, *MNRAS*, 455, L62
 Nixon C. 2015, *MNRAS*, 450, 2459
 Nixon C., King A.R., Price D., Frank J. 2012, *ApJ*, 757, 24
 Nixon C., Salvesen G. 2014, *MNRAS*, 437, 3994
 Ogilvie G.I. 1999, *MNRAS*, 304, 557
 Papaloizou J.C.B. & Pringle J.E. 1983, *MNRAS*, 202, 1983
 Pounds K.A., Reeves J.N., King A.R., Page K.L., O’Brien P.T., Turner M.J.L. 2003, *MNRAS*, 345, 705
 Pounds K.A. & Page K.L. 2006, *MNRAS*, 360, 1123
 Pounds K.A. & Reeves J.N. 2009, *MNRAS*, 397, 249
 Pounds K.A. 2014, *Space Science Rev.*, 183, 339
 Pounds K.A., Lobban A., Reeves J.N., Vaughan S.A. 2016a, *MNRAS*, 457, 2951 (P16)
 Pounds K.A., Lobban A., Reeves J.N., Costa M., Vaughan S.A. 2016b, *MNRAS*, 459, 4389

- Reeves J.N. et al. 2008, MNRAS, 385, L108
Shakura N.I. & Sunyaev R.A. 1973, A&A, 24, 337
Strueder L. et al. 2001, A&A, 365, L18
Tombesi F., Cappi M., Reeves J.N., Palumbo G.C., Yaqoob T.,
Braitto V., Dadina M. 2010, ApJ, 742, 44
Tombesi F., Cappi M., Reeves J.N., Palumbo G.C., Braitto V., Dad-
ina M. 2011, A&A, 521, A57